DOI 10.1007/s10812-020-01028-9
Journal of Applied Spectroscopy, Vol. 87, No. 3, July, 2020 (Russian Original Vol. 87, No. 3, May–June, 2020)

PHASE COMPOSITION, MICROSTRUCTURE, AND OPTICAL PROPERTIES OF Cu_2SnS_3 THIN FILMS

E. P. Zaretskaya,[a*] V. F. Gremenok,[a] V. A. Ivanov,[a] A. V. Stanchik,[a] O. M. Borodavchenko,[a] D. V. Zhyhulin,[b] S. Özçelik,[c] and N. Akçay[c]

UDC 539.26;538.913;548.736.5;539.216.2

The Cu_2SnS_3 (CTS) thin films were produced by deposition of Sn/Cu layers by RF sputtering followed by annealing in an Ar/S atmosphere with S and Sn sources. According to XRD analysis and Raman spectroscopy, it was shown that single-phase CTS films of a monoclinic structure with traces of the Cu_xS phase were formed at a temperature of 520°C. Scanning electron microscopy revealed a compact and homogeneous microstructure of the polycrystalline CTS layers. Photoluminescence spectra of the CTS films of monoclinic modification show one wide peak in the energy range of 0.7–1.0 eV, due to optical transitions of electrons from the conduction band to deep energy levels of acceptor-type defects.

Keywords: *solar cell, Cu_2SnS_3, thin film, crystal structure, Raman spectroscopy, photoluminecsence.*

Introduction. Significant progress in the photovoltaic industry is largely due to the development of thin-film solar cell (SC) technology. SCs based on absorbing layers of semiconductors based on the Cu–In–Ga–S(Se) (CIGS) system and its isoelectronic analogue Cu–Zn–Sn–S(Se) (CZTS) achieved an efficiency of 22.6 and 12.6% [1, 2]. However, the mass production of SCs based on CIGS and CZTS materials is limited by the complexity of obtaining an absorbing layer of homogeneous composition with structural ordering, as well as the high cost of rare elements In and Ga.

In the last decade, the direct-gap semiconductor Cu_2SnS_3 (CTS) has been actively studied as an alternative photoactive layer for inexpensive and nontoxic thin-film SCs. This material is well known as a side phase of the CZTS system, but has a wider range of chemical potential stability [3], which simplifies the control of the composition compared to the CZTS quaternary compound. Cu_2SnS_3 has an absorption coefficient of $\alpha > 10^4$ cm^{-1}, high *p*-type conductivity, and has a band gap in the range of 0.83–1.35 eV, depending on the structural modification [4–6]. The theoretically predicted efficiency of SC based on CTS is 30% [7]. However, due to deviation from stoichiometry and the presence of extraneous phases, an efficiency of 4.63% has been achieved [8, 9].

Like photoconverters based on CIGS and CZTS, the determining factor for increasing the conversion is controlling the growth and crystallization of the photoactive layer of Cu_2SnS_3. For the synthesis of Cu_2SnS_3 films, physical [10, 11] and chemical deposition methods are used, including the deposition of Cu/Sn, Sn/Cu/Sn metal packets (or CuS–SnS sulfides) in various sequences, followed by annealing in a sulfur (S) or hydrogen sulfide (H_2S) atmosphere [12–14]. The main problems in the formation of the photoactive layer of Cu_2SnS_3 are associated with the formation of a multiphase mixture of ternary compounds with different stoichiometry ($Cu_2Sn_3S_7$, Cu_3SnS_4, and Cu_4SnS_4) and polymorphic crystallization of Cu_2SnS_3 in various structures (tetragonal, cubic, monoclinic and triclinic) [5, 15–17].

The aim of this work is to study the phase composition, microstructural, and optical characteristics of Cu_2SnS_3 films formed by metal deposition in the Sn/Cu and Mo/Sn/Cu sequences by RF sputtering followed by sulfurization, and to select the optimal conditions for producing photoactive CTS layers for thin-film photoconverters.

*To whom correspondence should be addressed.

[a]State Scientific and Production Association, Scientific-Practical Materials Research Center of the National Academy of Sciences of Belarus, Minsk, 220072, Belarus; email: ezaret@physics.by; [b]JSC "INTEGRAL" — "INTEGRAL" Holding Managing Company, Minsk, 220108, Belarus; [c]Gazi University, Photonics Application & Research Center, Ankara, 06500, Turkey; email: sozcelik@gazi.edu.tr; neslihanakcay@baskent.edu.tr. Translated from Zhurnal Prikladnoi Spektroskopii, Vol. 87, No. 3, pp. 462–468, May–June, 2020. Original article submitted February 21, 2020.

 0021-9037/20/8703-0488

Experiment. *Formation of a CTS layer.* For the synthesis of a photoactive CTS layer, we used Sn/Cu metal layers deposited by RF sputtering on chemically clean glass substrates (SLG grade) and on substrates with a Mo film 300–800 nm thick. Metal deposition was carried out in the Sn/Cu sequence in an Ar atmosphere at a base pressure of 7.02×10^{-6} Torr and a substrate temperature of 25°C. The thickness of each layer is determined by the deposition time: 50 min for Sn and 80 min for Cu.

The CTS layer was synthesized in the reactor of a diffusion furnace with a temperature gradient of ≈0.1°C/cm in an inert gas Ar (N 6.0) 95%. The annealing system consisted of a specially designed graphite container for substrates with a volume of 12.5 cm^3 and solid-state sources of sulfur weighing 5–7 mg and tin weighing 15 mg. The reactor was preliminarily pumped out and filled with an inert gas Ar, then the reactor was re-pumped and filled with Ar to a pressure of 1 bar. At the first stage, the temperature was increased from room temperature to the temperature of sulfurization at a rate of 4°C/min. Two temperature regimes were used with a maximum crystallization temperature (T_1 = 520°C and T_2 = 550°C), which was held for 15 min, and then the furnace with the container was naturally cooled.

Research Methods. The phase composition and crystal structure of the synthesized CTS layers were studied by X-ray phase analysis (XRD) using a D8 Advance diffractometer (Bruker AXS, Germany) using CuK_α-radiation (λ = 0.1542 nm) with a filtered multilayer Ni–graphite monochromator with a tube voltage of 40 kV and a current of 40 mA. The microstructural characteristics of the films were studied using an H-800 scanning electron microscope (SEM) (Hitachi, Japan) with a resolution of 0.2 nm. The elemental composition of the synthesized films was determined by an INCA 350 energy dispersive X-ray microanalyzer (Oxford Instruments, United Kingdom) with a resolution of 1 μm^3 and a sensitivity of 0.1 at.%. The phases were identified by comparing experimentally determined interplanar distances *d* with JCPDS data (Joint Council for Power Diffraction Standards, 2013).

Raman spectra were recorded on a Nanofinder High End spectrometer. A solid-state laser with λ = 532 nm was used as an excitation source. The measurements were carried out at T_c = 20°C with reflection geometry in the range 150–2000 nm. Photoluminescence (PL) spectra were recorded using an MDR-23U diffraction monochromator equipped with a grating of 600 lines/mm (inverse linear dispersion 26 Å/mm). An InGaAs *p-i-n*-photodiode type G8370-03 (Hamamatsu, Japan) served as an optical signal detector. To excite luminescence, a diode laser module operating at λ ~ 405 nm with a power of <100 mW was used.

Results and Discussion. *Microstructure and phase composition of CTS films.* For the synthesis, precursors with the ratio Cu/Sn = 2.3 were used. The composition of the two synthesized series of CTS films, determined by energy dispersive X-ray spectroscopy (EDX), is given in Table 1. The main feature of the composition of films synthesized at the same temperatures on different substrates is a significant excess of the concentration of copper in the synthesis on glass substrates. The Cu/Sn ratio for the CTS sample No. 10 synthesized on glass at 520°C is 3.70, and for the Mo/CTS sample No. 11 (synthesized on a substrate with a molybdenum layer) the ratio Cu/Sn = 2.52. Similarly, for the CTS sample No. 12 formed on glass at T_g = 550°C, the ratio Cu/Sn = 4.14, while for the Mo/CTS sample No. 11 the ratio is 3.16. The observed effect may be due to the difference in the thermal conductivity of glass and molybdenum, affecting the kinetics of phase formation and the growth of CTS material. Since the thermal conductivity of molybdenum is ~500 times higher than glass, heat transfer from the Mo layer at the Mo/Sn/Cu heterointerface provides a higher interaction rate of Cu_xSn_y binary intermetallic compounds with sulfur and, accordingly, reduces tin losses. Further research is needed to confirm this assumption.

An increase in the recrystallization temperature from T_g = 520°C to 550°C is accompanied by an increase in the concentration of copper during synthesis on both types of substrates due to re-evaporation of the highly volatile tin sulfides Sn_xS_y. In this case, the total ratio of the components in the cationic sublattice to the sulfur content in the anionic sublattice (Cu + Sn)/S for all synthesized CTS layers slightly exceeds the stoichiometric ratio.

The CTS films obtained as a result of annealing are uniform, have no visible punctures, and have high adhesion to the substrate. Fig. 1 shows an SEM image of a cleaved CTS layer on a glass substrate and a CTS layer synthesized on a substrate with a Mo sublayer at various sulfurization temperatures. CTS, a material synthesized on an amorphous glass substrate at T_g = 520°C (Fig. 1a), consists of an agglomerate of densely fused crystallites with no visible grain boundaries. CTS material synthesized on a substrate with a Mo layer at the indicated temperature differs in the presence of an intermediate layer with a thickness of 400 nm, consisting of fine crystallites and caused by significant mismatch between the lattice of the CTS layer and Mo (*a* = 3.147 Å) (Fig. 1b).

An increase in the sulfurization temperature to T_g = 550°C during the synthesis of the CTS layer on both types of substrates is accompanied by the growth of Cu-enriched crystallites both in the vertical direction and parallel to the frontal surface, reaching sizes of 685 × 1000 nm. In the vertical direction, the crystallite size is comparable with the thickness of

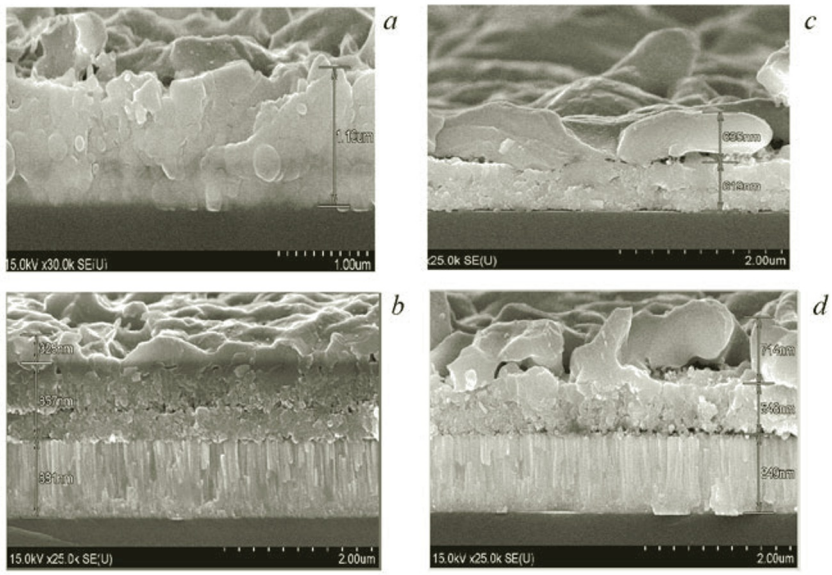

Fig. 1. SEM images of a transverse cleavage of CTS films on a glass substrate [No. 10 (a), 12 (c)] and a substrate with a Mo sublayer [No. 9 (b), 11 (d)] at temperatures T_g = 520 (a, b) and 550°C (c, d).

TABLE 1. Elemental Composition (at.%) of CTS Films on a Glass Substrate and a Substrate with a Mo Sublayer

T_g, °C	Sample	Cu	Sn	S	Mo	Cu/Sn	(Cu + Sn)/S
520	No. 9, Mo/CTS	36.66	14.54	39.80	4.12	2.52	1.43
	No. 10, CTS	41.03	11.60	42.37	–	3.70	1.23
550	No. 11, Mo/CTS	39.35	12.42	41.40	1.83	3.16	1.25
	No. 12, CTS	41.93	9.99	41.58	–	4.14	1.23

the deposited layer 635–714 nm (Fig. 1c, e), which reduces the recombination at the grain boundaries and is an important condition for the creation of instruments [18]. However, the growth and isolation of such copper enriched crystallites as a separate fraction in the course of further synthesis of the optical absorber leads to the synthesis of a CTS film with copper shunting protrusions and is an undesirable factor.

When studying the phase composition of all CTS and Mo/CTS films obtained under the indicated conditions, the formation of the Cu_2SnS_3 compound with monoclinic structure, which was observed for the annealing temperature of 550°C, was established [3]. Radiographs of the films contain the main reflections of the compound Cu_2SnS_3 with monoclinic structure (JCPDS No. 1526187), low intensity reflections of $Cu_{1.78}S$ copper sulfide (JCPDS No. 1528226) and for films deposited on glass/Mo, the reflection at 40.27° from the Mo contact. Figure 2 shows X-ray diffraction patterns for films with Cu/Sn = 2.52 (No. 9, Mo/CTS) and Cu/Sn = 3.70 (No. 10, CTS).

The position of the main reflection at 28.37° for the CTS layer with the ratio Cu/Sn = 2.52 (sample No. 9) slightly shifts to 28.40° with an increase in the copper content (Cu/Sn = 3.70, No. 10), which indicates a decrease in the interplanar distance *d* and lattice parameters.

Table 2 shows the calculated lattice parameters for the CTS and Mo/CTS layers obtained by the Foolproof method using the MAUD (Materials Analysis Using Diffraction) program [18–20]. Despite significant deviations from the stoichiometric composition of the synthesized films, the lattice parameters obtained are in good agreement with the published data for the monoclinic modification of CTS [16], which is consistent with a wide range of stability of the chemical potential of the CTS compound in the Cu–Sn–S system [21]. Nevertheless, the unambiguous identification of a number of phases and

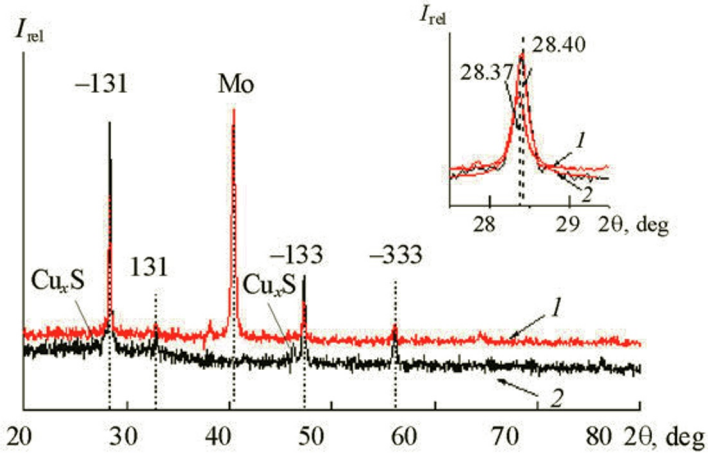

Fig. 2. Experimental X-ray diffraction patterns for glass/Mo/CTS (No. 9) (1) and glass/CTS (No. 10) (2) samples synthesized at T_g = 520°C.

TABLE 2. Calculated Lattice Parameters for CTS and Mo/CTS Layers

Sample	Phase	*a*, Å	*b*, Å	*c*, Å	β, deg
No. 10, CTS	Cu_2SnS_3	6.65(36)	11.55(05)	6.65(47)	109.30(00)
	$Cu_{1.78}S$	5.55(12)	–	–	–
No. 9, Mo/CTS	Cu_2SnS_3	6.66(73)	11.54(46)	6.66(83)	109.60(56)
	$Cu_{1.78}S$	5.55(120	–	–	–
	Mo	3.15(55)	–	–	–
Cu_2SnS_3 (1526187)		6.653	11.537	6.665	109.39
$Cu_{1.78}S$ (1528226)		5.582	–	–	–
Mo (4001308)		3.14683	–	–	–

their crystal structure, including cubic CTS (JCPDS 01-089-2877), tetragonal CTS (JCPDS No. 1526187), is difficult on the basis of the XRD data due to the overlapping of diffraction peaks.

Raman spectroscopy of CTS thin films. In order to correctly determine the phase composition of CTS films obtained at various synthesis temperatures, confocal Raman spectroscopy was used. According to XRD, the dominant phase in the obtained layers is the monoclinic structure phase with stoichiometry of Cu_2SnSe_3. A monoclinic structure with a space group (*Cc*) is characterized by an irreducible representation $\Gamma = 3A^{I} \ldots 3A^{II}$ with six active Raman and IR modes [21, 22]. Usually, two dominant peaks are observed in this system, attributed to symmetry modes *A*, including the vibration of anions: 290 cm^{-1} — A^{I}, Γ1 [W1], 314–317 cm^{-1} — A^{I} [22].

To verify the uniformity of the phase composition, Raman spectra were recorded at five randomly selected points on the surface of the sample. The phase composition of the films was determined. Typical experimental Raman spectra of the studied CTS are shown in Fig. 3. The position of the peaks in the Raman spectra is determined by approximating the data by the Lorentz functions. In the presented Raman spectra, the most intense vibrations appear due to the A^{I}, Γ1 [W1] modes at 293 cm^{-1} and the second-order modes A^{I} at 352 cm^{-1} of the monoclinic Cu_2SnS_3 phase observed in CTS films [13–16, 23]. However, the contribution from vibrations of other phases cannot be completely excluded. The low-intensity oscillation at 267 cm^{-1} is associated with the phase of copper sulfide $Cu_{2-x}S$ (268 cm^{-1}), revealed by studying the phase composition by the XRD method. Modes at 267 and 304 cm^{-1} can also be attributed to vibrations of the Cu_2SnS_3 phase of a cubic structure. In the Raman spectra of Mo/CTS films, there is an oscillation with a maximum at 386 cm^{-1}, the intensity of which changes significantly when the beam scans along surface points. Considering that the penetration depth of the laser beam

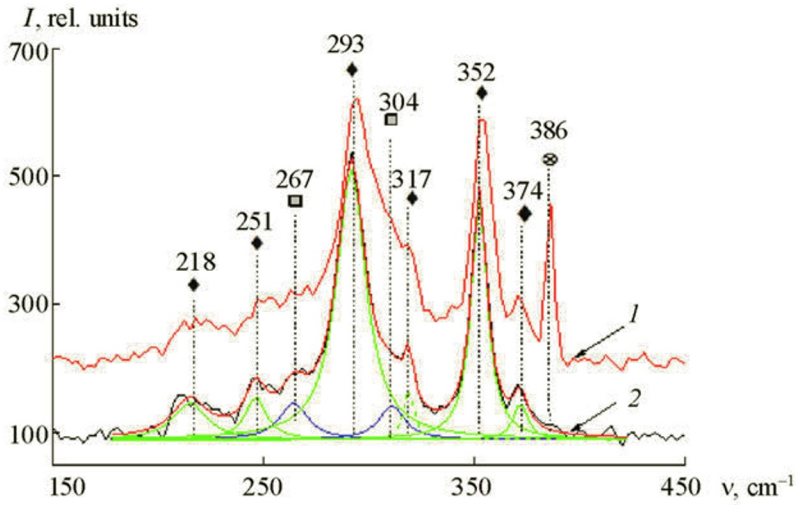

Fig. 3. Raman spectra of Mo/CTS (No. 9) (1) and CTS (No. 10) (2) samples synthesized at T_g = 520°C (♦ — reflections of the monoclinic structure, □ — reflections of the cubic structure).

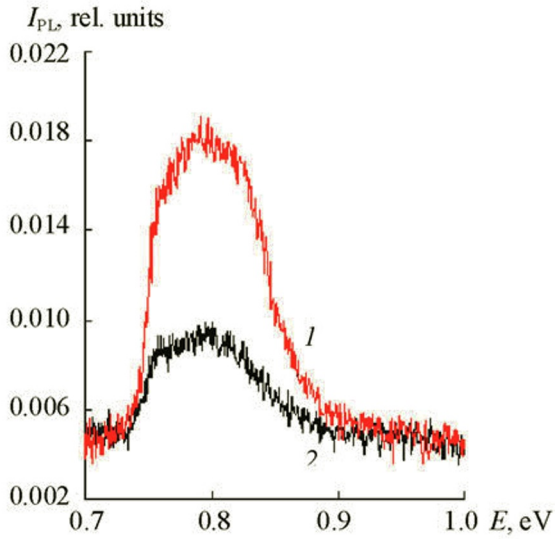

Fig. 4. PL spectra recorded at T ~ 78 K for CTS films synthesized at T_g = 520 (No. 10) (1) and 550°C (No. 12) (2).

for semiconductors with a high optical absorption coefficient (×10^4 cm^{-1}) is estimated to be ~200–250 nm, the vibration at 386 cm^{-1} can be attributed to the E_{2g}^1 mode of the molybdenum sulfide phase MoS_2 [24] in the transition region of Mo/CTS, which manifests due to the presence of through pores in the synthesized CTS layer.

Photoluminescence of CTS films. Optical transitions for the CTS compound of various polymorphic modifications are in the range 0.83–1.35 eV, which was studied to identify the type of structures formed in the synthesized material. The luminescence spectra were recorded at liquid nitrogen temperature (78 K) with direct immersion of samples in a cooling liquid.

Typical PL spectra at T ~ 78 K for CTS thin films synthesized on a glass substrate at T_g = 520°C (No. 10) and T_g = 550°C (No. 12) are shown in Fig. 4. As can be seen, for each sample, only one wide emission band appears in the range 0.7–1.0 eV. A sharp decrease in the band intensity in the energy range of <0.75 eV is due to the spectral sensitivity of the InGaAs detector for optical signals. The emission maxima correspond to energies of ~0.798 and ~0.792 eV for samples No. 10 and No. 12. The estimated half-width of the PL bands ~0.105 eV is approximately the same for both samples. As

is known, the band gap for direct interband transitions in the Cu_2SnS_3 compound with monoclinic symmetry of the crystal lattice according to optical measurements is ~0.91–0.95 eV [25–28]. The detection of exciton luminescence and E_g ~ 0.94 eV should be considered the most correct data [28]. Considering this and the low luminescence intensity, low energy position of the PL bands and their large half-width of ~ 0.105 eV, it can be assumed that the appearance of these bands is due to optical transitions of electrons from the conduction band to deep energy levels of acceptor-type defects with an activation energy of 0.14–0.15 eV. Since the ratios of the components in the cationic to anionic sublattices are the same for these samples (Cu + Sn)/S = 1.23, the low intensity of the emission band of sample No. 12 can be due to a higher concentration of defects in its cationic sublattice Cu/Sn = 4.14 compared to CTS layer with Cu/Sn = 3.70 (No. 10). Based on the studies, it can be concluded that the optimum temperature for the synthesis of CTS layers of a monoclinic structure with radiative properties in the visible region of the spectrum is an annealing temperature of 520^{o}C.

Conclusions. A method is described for the synthesis of monoclinic Cu_2SnS_3 films by reactive diffusion of chalcogen S into intermetallic Sn/Cu layers at temperatures around 520^{o}C. Complex studies of the phase composition, microstructural and optical characteristics of the synthesized Cu_2SnS_3 layers were carried out. Correlations between the characteristics and optical properties of Cu_2SnS_3 films with synthesis modes are established. The obtained material of the Cu_2SnS_3 layers is characterized by emissive properties in the visible region of the spectrum, which satisfies the requirements for use as an absorbing layer in thin-film photoconverters. The advantage of the proposed method is the possibility of eliminating the preliminary stage of annealing of Cu/Sn precursor layers used to form Cu_xSn_y intermetallic compounds from the technological cycle. The described procedure can be easily adapted to industrial technologies in connection with the use of well-known deposition methods, such as magnetron sputtering and low annealing temperatures for the crystallization process.

Acknowledgments. The studies were funded by the Belarusian Republican Foundation for Fundamental Research (Grant No. F18TYuB-006) and the Turkish Scientific and Technical Research Council TUBITAK (TR) (Grant No. 118 F009).

REFERENCES

1. P. Jackson, R. Wuerz, D. Hariskos, E. Lotter, W. Witte, and M. Powalla, *Phys. Status Solidi — Rapid Res. Lett.*, **10**, 583–586 (2016).
2. W. Wang, M. T. Winkler, O. Gunawan, T. Gokmen, T. K. Todorov, Y. Zhu, and D. B. Mitzi, *Adv. Energy Mater.*, **4**, 1301465(1–5) (2014).
3. M. Onoda, X. Chen, A. Sato, and H. Wada, *Mater. Res. Bull.*, **35**, 1563–1570 (2000).
4. D. Avellaneda, M. T. S. Nair, and P. K. Nair, *J. Electrochem. Soc.*, **157**, D346–D352 (2010).
5. N. Aihara, H. Araki, A. Takeuchi, K. Jimbo, and H. Katagiri, *Phys. Status Solidi*, **10**, 1086–1091 (2013).
6. P. A. Fernandes, P. M. P. Salomé, and A. F. da Cunha, *J. Phys. D: Appl. Phys.*, **43**, 215403 (2010).
7. A. Kuku and O. A. Fakolujo, *Sol. Energy Mater.*, **16**, 199–204 (1987).
8. A. Kanai, K. Toyonaga, K. Chino, H. Katagiri, and H. Araki, *Jpn. J. Appl. Phys.*, **54**, 08KC06(1–4) (2015).
9. M. Nakashima, J. Fujimoto, T. Yamaguchi, and M. Izaki, *Appl. Phys. Express*, **8**, 042303(1–4) (2015).
10. A. C. Lokhande, R. B. V Chalapathy, M. He, E. Jo, M. Gang, S. A. Pawar, C. D. Lokhande, and J. H. Kim, *Sol. Energy Mater. Sol. Cells*, **153**, 84–107 (2016).
11. R. Chierchia, F. Pigna, M. Valentini, C. Malerba, E. Salza, P. Mangiapane, T. Polichetti, and A. Mittiga, *Phys. Status Solidi Curr. Top. Solid State Phys.*, **13**, 35–39 (2016).
12. D. Tiwari, T. K. Chaudhuri, T. Shripathi, U. Deshpande, and V. G. Sathe, *Appl. Phys. Mater. Sci. Process.*, **117**, 1139–1146 (2014).
13. D. Tiwari, T. K. Chaudhuri, T. Shripathi, U. Deshpande, and R. Rawat, *Sol. Energy Mater. Sol. Cells*, **113**, 165–170 (2013).
14. J. Li, J. Huang, Y. Zhang, Y. Wang, C. Xue, G. Jiang, W. Liu, and C. Zhu, *RSC Adv.*, **6**, 58786–58795 (2016).
15. H. Dahman and L. El Mir, *J. Mater. Sci. Mater. Electron.*, **26**, 6032–6039 (2015).
16. J. Han, Y. Zhou, Y. Tian, Z. Huang, X. Wang, J. Zhong, Z. Xia, B. Yang, H. Song, and J. Tang, *Front. Optoelectron.*, **7**, 37–45 (2014).
17. T. K. Todorov, J. Tang, S. Bag, O. Gunawan, T. Gokmen, Y. Zhu, and D. B. Mitzi, *Adv. Energy Mater.*, **3**, 34–38 (2013).
18. M. Ferrari and L. Lutterotti, *J. Appl. Phys.*, **76**, No. 11, 7246–7255 (1994).
19. H.-R. Wenk, S. Matthies, and L. Lutterotti, *Mater. Sci. Forum*, **157–162**, 473–480 (1194).
20. L. Lutterotti, S. Matthies, H.-R. Wenk, A. J. Schultz, and J. Richardson, *J. Appl. Phys.*, **81**, No. 2, 594–600 (1997).

21. Pawel Zawadzki, Lauryn L. Baranowski, Haowei Peng, Eric S. Toberer, David S. Ginley, William Tumas, Andriy Zakutayev, and Stephan Lany, *Appl. Phys. Lett.*, **103**, No. 25, 253902 (2013).
22. G. Marcano, C. Rincón, S. A. López, G. Sánchez Pérez, J. L. Herrera-Pérez, J. G. Mendoza-Alvarez, and P. Rodríguez, *Solid State Commun.*, **151**, No. 1, 84–86 (2011).
23. G. E. Delgado, A. J. Mora, G. Marcano, and C. Rincón, *Mater. Res. Bull.*, **38**, 1949–1953 (2003).
24. T. J. Wieting and J. L. Verble, *Phys. Rev. B*, **3**, 4286–4292 (1971).
25. J. de Wild, E. Kalesaki, L. Wirtz, and P. J. Dale, *Phys. Status Solidi RRL*, **11**, 1600410 (2017).
26. A. Crovetto, R. Chen, R. B. Ettlinger, A. C. Cazzaniga, J. Schou, C. Persson, and O. Hansen, *Sol. Energy Mater. Sol. Cells*, **154**, 121–129 (2016).
27. N. Aihara, Y. Matsumoto, and K. Tanaka, *Appl. Phys. Lett.*, **108**, 092107 (2016).
28. T. Raadik, M. Grossberg, J. Krustok, M. Kauk-Kuusik, A. Crovetto, R. Bolz Ettinger, O. Hansen, and J. Schou, *Appl. Phys. Lett.*, **110**, 261105 (2017).